JOURNAL OF COMPUTATIONAL PHYSICS 84, 377–402 (1989)

The Numerical Solution of Parabolic Free Boundary Problems Arising from Thin Film Flows

ROLAND HUNT

Department of Mathematics,
University of Strathclyde, Glasgow, Scotland

Received December 8, 1987; revised October 3, 1988

A numerical solution of high accuracy is obtained for the large Reynolds number, thin film flow over a horizontal flat plate, cylinders and spheres resulting from a vertical jet of liquid falling on the surface. A coordinate transformation is used which simultaneously maps the film thickness onto the unit interval and removes the singularity at the leading edge. The resulting equations are parabolic and these are solved using the Keller box method which is modified to accommodate the outer, free boundary. Using an extrapolation technique, results of sixth order accuracy are obtained with an estimated accuracy of six significant figures. For the flat plate, solutions for both 2-dimensional and axisymmetric jets are obtained and, for cylinders and spheres, different Froude numbers and volume flows are considered. The method can be used to solve any parabolic problem with a free boundary. © 1989 Academic Press, Inc.

1. INTRODUCTION

Liquid thin films occur in a variety of industrial contexts. A common example is the thin film of running water surrounding horizontal heat exchanger pipes in steam condensers. This water arises from the condensed steam and significantly affects the heat transfer characteristics of the tubes. Similar liquid films occur in absorbers and evaporators of the chemical engineering industry. In order to understand the operation and, in particular, the efficiency of these processes it is important to have a detailed study of the flow in such firms.

We shall be concerned with the large Reynolds number case for which the governing equations are the boundary layer equations with a free surface. Many such flows [1–6] have been solved, usually using the Pohlhausen integral momentum technique [7] which assumes an approximate velocity profile across the thickness of the film. In this paper an accurate numerical solution is obtained against which such solutions can be tested. Our primary aim here, however, in a description of how the numerical solution is obtained; the detailed comparison with this theoretical work is fully discussed in another paper [8].

Specifically we consider the following four cases:

(a) a 2-dimensional jet falling vertically onto a flat surface [1],

(b) a 2-dimensional jet falling vertically onto the top generator of a cylinder [6],

0021-9991/89 $3.00
Copyright © 1989 by Academic Press, Inc.
All rights of reproduction in any form reserved.

(c) an axisymmetric jet falling vertically onto a flat surface [1], and

(d) an axisymmetric jet falling vertically onto the upper pole of a sphere [5].

Each of these cases has a flow which is initially Blasius and with an outer boundary which is a free surface. To prepare the governing equations for accurate numerical computation it is necessary to use a transformation which removes the Blasius singularity and it is advantageous if the free surface is mapped onto a fixed outer boundary [9]. These transformations are straightforward and well known when applied separately but here we need to apply them simultaneously which involves a more general transformation. Such a transformation only becomes tractable by writing the equations as a first-order system and making use of the form that the governing equations take. This transformation is described in Section 3.

The Keller box method [8, 9] incorporating extrapolation has proved very successful in obtaining results of high accuracy for parabolic boundary layer type equations [10–16]. Section 4 describes how this method is modified to incorporate the free boundary. The results and their accuracy are discussed in Section 5, together with our main conclusions.

2. Governing Equations

(a) *Two-Dimensional Flat Plate*

In Fig. 1(a) is depicted a 2-dimensional flow in which a thin jet of width $2H_0$ plunges vertically with velocity U_0 onto a horizontal flat plate. By symmetry the flow separates equally to either side and we will be concerned with the flow to the right of A immediately after the point at which the flow is essentially horizontal. Since we are considering the large Reynolds number case in which the flow is confined to a thin film, we may neglect vertical velocities in comparison with horizontal and X derivatives in comparison with Y in the Navier–Stokes equations (where X and Y are the horizontal and vertical coordinates respectively). The resulting governing equations become very similar to the boundary layer equations and are

$$\begin{gathered} \frac{\partial U}{\partial X}+\frac{\partial V}{\partial Y}=0 \\ U\frac{\partial U}{\partial X}+V\frac{\partial U}{\partial Y}+\frac{1}{\rho}\frac{\partial p}{\partial X}=\nu\frac{\partial^2 U}{\partial Y^2} \\ \frac{\partial p}{\partial Y}=0 \end{gathered} \tag{1}$$

where U, V, ρ, p, and ν are the horizontal and vertical velocities, density, pressure, and kinematic viscosity, respectively. The third equation shows that p is a function

of X alone and, if we assume the pressure to be constant outside the firm, this implies that it is constant thoughout the film. Equations (1) then simplify to

$$\frac{\partial U}{\partial X}+\frac{\partial V}{\partial Y}=0$$
$$U\frac{\partial U}{\partial X}+V\frac{\partial U}{\partial Y}=\nu\frac{\partial^2 U}{\partial Y^2} \tag{2}$$

which are subject to the boundary conditions

$$U=V=0 \qquad \text{on} \quad Y=0$$
$$\frac{\partial U}{\partial Y}=0 \qquad \text{on} \quad Y=H(X),\ X>0, \tag{3}$$

where the first of these is the no-slip condition and the second assumes no shear on the free surface and $H(X)$ is the film thickness. Conservation of mass demands

$$\int_0^{H(X)} U\,dY=\text{constant}=H_0U_0. \tag{4}$$

As the fluid turns the corner from vertical to horizontal flow, the flow is essentially inviscid since the boundary layer has not yet developed (see [8]). We may then use Bernouilli's equation $p+\frac{1}{2}\rho U^2=\text{constant}$ along a streamline and since both p and ρ are constant we deduce that the initial condition is

$$U=U_0, \qquad V=0 \qquad \text{on} \quad X=0,\ 0<Y<H(X). \tag{5}$$

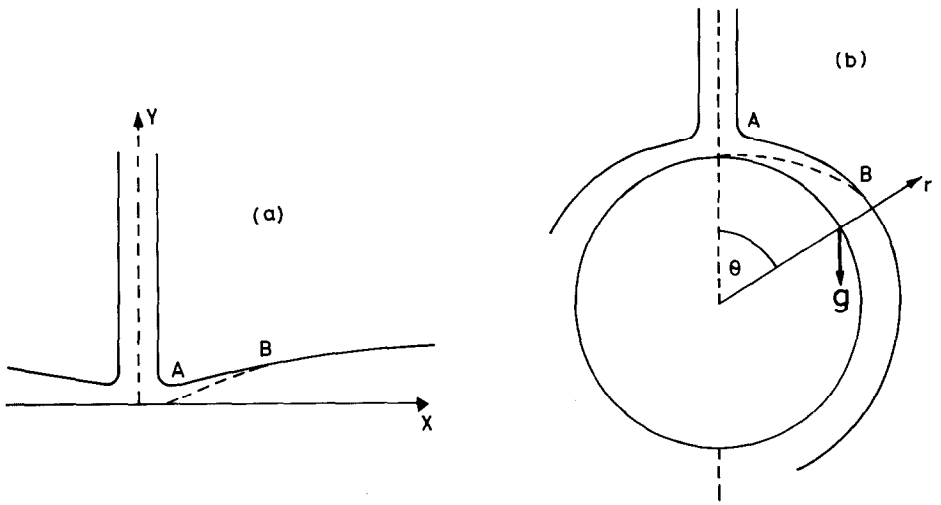

FIG. 1. The vertical jet and resulting film for (a) the flat plate and (b) the cylinder or sphere. The dotted curve AB indicates the growing boundary layer.

Equations (2) can be satisfactorily nondimensionalised by

$$X = RH_0 x, \qquad Y = H_0 y, \qquad H = H_0 h$$
$$U = U_0 u, \qquad V = \frac{U_0}{R} v, \tag{6}$$

where $R = U_0 H_0/\nu$ is the jet Reynolds number. The problem then becomes

$$\frac{\partial u}{\partial x} + \frac{\partial v}{\partial y} = 0$$
$$u\frac{\partial u}{\partial x} + v\frac{\partial u}{\partial y} = \frac{\partial^2 u}{\partial y^2} \tag{7}$$

subject to

$$u = v = 0 \qquad \text{on} \quad y = 0$$
$$\frac{\partial u}{\partial y} = 0 \qquad \text{on} \quad y = h(x) \tag{8}$$
$$u = 1, \qquad v = 0 \qquad \text{on} \quad x = 0,\ 0 < y < h(x)$$

with integral constraint (4) yielding

$$\int_0^{h(x)} u\, dy = 1. \tag{9}$$

(b) *Cylinder*

For the cylinder (Fig. 1(b)) the vertical jet is the same as for the flat plate having width $2H_0$ and velocity U_0. Using the Navier–Stokes equations in cylindrical polar coordinates including a vertical gravitational force term and assuming that the film thickness is thin, the govening equations equivalent to Eqs. (2) are

$$\frac{\partial v_r}{\partial r} + \frac{1}{a}\frac{\partial v_\theta}{\partial \theta} = 0$$
$$v_r\frac{\partial v_\theta}{\partial r} + \frac{v_\theta}{a}\frac{\partial v_\theta}{\partial \theta} = g\sin\theta + \nu\frac{\partial^2 v_\theta}{\partial r^2}, \tag{10}$$

where v_r, v_θ, g and a are the velocities in the r and θ directions, the acceleration due to gravity, and the radius of the cylinder, respectively. The conservation of mass integral constraint is

$$\int_a^{a + H(\theta)} v_\theta\, dr = U_0 H_0. \tag{11}$$

These equations are non-dimensionalised using

$$\theta = x, \qquad r = a + \frac{a}{R_e^{1/2}} y, \qquad H = \frac{a}{R_e^{1/2}} h$$
$$v_\theta = U_0 u, \qquad v_r = \frac{U_0}{R_e^{1/2}} v, \tag{12}$$

where $R_e = U_0 a/\nu$ is the Reynolds number, giving

$$\frac{\partial u}{\partial x} + \frac{\partial v}{\partial y} = 0$$
$$u \frac{\partial u}{\partial x} + v \frac{\partial u}{\partial y} = \frac{1}{F} \sin x + \frac{\partial^2 u}{\partial y^2} \tag{13}$$

subject to the integral constraint

$$\int_0^{h(x)} u \, dy = \gamma_c \tag{14}$$

and the same boundary conditions (8) as the flat plate. Here $F = U_0^2/ga$ is the Froude number and $\gamma_c = R_e^{1/2} H_0/a$.

(c) *Axisymmetric Flat Plate*

In this case we have a cylindrical jet of radius H_0 and velicity U_0 plunging vertically onto a flat plate. Equations (2) in cylindrical polar coordinates are

$$\frac{1}{r} \frac{\partial}{\partial r} (r u_r) + \frac{\partial u_z}{\partial z} = 0$$
$$u_r \frac{\partial u_r}{\partial r} + u_z \frac{\partial u_r}{\partial z} = \nu \frac{\partial^2 u_r}{\partial z^2} \tag{15}$$

with integral constraint

$$\int_0^{H(r)} r u_r \, dz = \tfrac{1}{2} H_0^2 U_0 \tag{16}$$

where r, z, u_r, and u_z are the radial and vertical coordinates and corresponding velocities, respectively. These may be non-dimensionalised by

$$r = R^{1/3} x, \qquad z = R^{-1/3} y, \qquad H = R^{-1/3} h$$
$$u_r = U_0 u, \qquad u_z = \frac{U_0}{R^{2/3}} v \tag{17}$$

to give

$$\frac{1}{x}\frac{\partial}{\partial x}(xu)+\frac{\partial v}{\partial y}=0$$
$$u\frac{\partial u}{\partial x}+v\frac{\partial u}{\partial y}=\frac{\partial^2 u}{\partial y^2} \tag{18}$$

and integral constraint

$$\int_0^{h(x)} xu\,dy=\tfrac{1}{2}, \tag{19}$$

again subject to the boundary conditions (8).

(d) *Sphere*

In this case a cylindrical jet (radius H_0 and velocity U_0) impinges onto the top of a sphere. In this geometry the first of equations (10) and integral constraint (11) become

$$\frac{\partial v_r}{\partial r}+\frac{1}{a\sin\theta}\frac{\partial}{\partial\theta}(v_\theta\sin\theta)=0$$
$$a\sin\theta\int_a^{a+H(\theta)} v_\theta\,dr=\tfrac{1}{2}H_0^2U_0 \tag{20}$$

with the second of equations (10) being unchanged. These are non-dimensionalised using (12) to give

$$\frac{\partial}{\partial x}(u\sin x)+\frac{\partial}{\partial y}(v\sin x)=0$$
$$u\frac{\partial u}{\partial x}+v\frac{\partial u}{\partial y}=\frac{1}{F}\sin x+\frac{\partial^2 u}{\partial y^2} \tag{21}$$

with integral constraint

$$\int_0^{h(x)} u\,dy=\gamma_s, \tag{22}$$

where $\gamma_s=\frac{1}{2}R_e^{1/2}H_0^2/U_0^2$ and subject to boundary conditions (8).

For each of the four problems we eliminate the continuity equation by introducing a stream function ψ defined by

$$u=G(x)\frac{\partial\psi}{\partial y},\qquad v=-G(x)\frac{\partial\psi}{\partial x} \tag{23}$$

where $G(x)$ equals (a) 1, (b) 1, (c) $1/x$, and (d) $1/\sin x$ for the four cases. Owing to the geometry $h(x)$ is singular at $x=0$ in case (c) and at $x=0$ and π in case (d). To remove this singularity we introduce $\bar{y}$ and $\bar{h}(x)$ given by

$$y = G(x)\,\bar{y}, \qquad h = G(x)\bar{h}. \tag{24}$$

Substituting euations (23) and (24) into (7), (13), (18), and (21) gives

$$\begin{aligned}
&\text{(a)} \quad \psi_{\bar{y}\bar{y}\bar{y}} = \psi_{\bar{y}}\psi_{x\bar{y}} - \psi_x\psi_{\bar{y}\bar{y}} \\
&\text{(b)} \quad \psi_{\bar{y}\bar{y}\bar{y}} + (1/F)\sin x = \psi_{\bar{y}}\psi_{x\bar{y}} - \psi_x\psi_{\bar{y}\bar{y}} \\
&\text{(c)} \quad \psi_{\bar{y}\bar{y}\bar{y}} = (1/x^2)(\psi_{\bar{y}}\psi_{x\bar{y}} - \psi_x\psi_{\bar{y}\bar{y}}) \\
&\text{(d)} \quad \psi_{\bar{y}\bar{y}\bar{y}} + (1/F)\operatorname{cosec} x = \operatorname{cosec}^2 x(\psi_{\bar{y}}\psi_{x\bar{y}} - \psi_x\psi_{\bar{y}\bar{y}})
\end{aligned} \tag{25}$$

subject to boundary conditions

$$\begin{aligned}
&\psi = 0, \quad \psi_{\bar{y}} = 0 \quad \text{on} \quad \bar{y} = 0 \\
&\psi = \gamma, \quad \psi_{\bar{y}\bar{y}} = 0 \quad \text{on} \quad \bar{y} = \bar{h}(x),\ x > 0 \\
&\psi = \bar{y}, \quad \bar{h} = \gamma \quad \text{on} \quad x = 0,\ 0 < \bar{y} < \bar{h}(x),
\end{aligned} \tag{26}$$

where γ equals (a) 1, (b) γ_c, (c) $\frac{1}{2}$, and (d) γ_s. Here $\psi = \gamma$ on $\bar{y} = \bar{h}(x)$ is the integral constraint and $\bar{h} = \gamma$ at $x = 0$ sets the initial film thickness consistent with this constraint. In the next two sections we will be concerned with the numerical solution of Eqs. (25) subject to (26).

3. Transformation of the Equations

There many numerical techniques for solving free boundary problems [9]. The simplest approach would be to use a fixed grid in which the position of the free boundary is "tracked" as the calculation proceeds. However, such a method can be inaccurate and a more satisfactory approach would be to transform the domain onto a rectangle. This is the technique we seek to use here, adapted so as to remove the boundary layer inconsistency at leading edge. From (26) we see that the boundary conditions $\psi_{\bar{y}} = 1$ at $x = 0$ and $\psi_{\bar{y}} = 0$ at $\bar{y} = 0$ for $x > 0$ are inconsistent, and this is usually removed by making the Blasius transformation $y = x^{1/2}\eta$, $\psi = x^{1/2}f$. However, this is unsatisfactory in our case since in (x, η) coordinates as $x \to 0$ the outer boundary $\bar{y} = \bar{h}(x)$ would have infinite extent and be difficult to cope with numerically. Hence, we will use a more general transformation which will

keep the essential features of the Blasius transformation and at the same time have the outer boundary at a finite distance.

To illustrate this transformation we will consider the cylindrical case (b) and anticipating using the Keller box method to integrate the equations we write the second of equations (25) as the first-order system

$$\begin{aligned} \psi_{\bar{y}} &= u \\ u_{\bar{y}} &= w \\ w_{\bar{y}} + \frac{1}{F}\sin x &= uu_x - w\psi_x. \end{aligned} \tag{27}$$

We transform from $(x, \bar{y})$ variables to (ξ, η) variables using

$$\bar{y} = \bar{y}(\xi, \eta), \qquad x = x(\xi). \tag{28}$$

The dependent variables are transformed as

$$\psi = grf, \qquad u = r\bar{u}, \qquad w = \frac{r}{g}\bar{w}, \tag{29}$$

where r and g can depend on both ξ and η. Changing the order, Eqs. (27) then become

$$\begin{aligned} &\bar{w}_\eta + \left(\frac{r_\eta}{r} - \frac{g_\eta}{g}\right)\bar{w} - \frac{sgr_\xi}{x'}\bar{u}^2 + \frac{s(gr)_\xi}{x'}f\bar{w} + \frac{1}{F}\frac{gs}{r}\sin(x(\xi)) = \frac{srg}{x'}(\bar{u}\bar{u}_\xi - \bar{w}f_\xi) \\ &f_\eta = \frac{s}{g}\bar{u} - \left(\frac{g_\eta}{g} + \frac{r_\eta}{r}\right)f, \qquad \bar{u}_\eta = \frac{s}{g}\bar{w} - \frac{r_\eta}{r}\bar{u}, \end{aligned} \tag{30}$$

where $s = \partial\bar{y}/\partial\eta$ and $' \equiv d/d\xi$. Using (29) rather than a more general case causes the right-hand side of the third of Eqs. (27) to be transformed without involving terms containing $\bar{y}_\xi$. The exclusion of $\bar{y}_\xi$ and regarding the governing equations as a first-order system has considerably simplified the algebra which otherwise would be untractable.

A suitable transformation for $\bar{y}$ in Eq. (28) should map the interval $0 \leqslant \bar{y} \leqslant \bar{h}$ onto $0 \leqslant \eta \leqslant 1$ and for small ξ it should mimic the Blasius transformation $\bar{y} = \eta x^{1/2}$. A simple transformation which has these properties is

$$\bar{y} = \frac{\xi\eta\bar{h}}{\xi + 1 - \eta}, \qquad x = \xi^2 \tag{31}$$

where the second of Eqs. (31) anticipates that variables near the leading edge vary as $x^{1/2}$. In the Blasius transformation (with r set to unity), $g=\xi$, but this is unsatisfactory since $f\to\infty$ as $\xi\to 0$ and instead we choose g to be

$$g=\frac{\xi}{\xi+1-\eta}. \tag{32}$$

Using Eqs. (31) and (32) with $r=1$, Eqs. (30) become

$$\bar{w}_\eta-\frac{1}{\xi+1-\eta}\bar{w}+\alpha t\frac{(1-\eta)}{\xi+1-\eta}f\bar{w}+\alpha\beta t\bar{u}^2+\frac{t}{2F}(2-\beta)\,\xi^{1/\alpha}\sin(\xi^{1/\alpha})$$
$$=\alpha t\xi(\bar{u}\bar{u}_\xi-\bar{w}f_\xi) \tag{33a}$$

$$f_\eta=\frac{\bar{h}(1+\xi)}{\xi+1-\eta}\bar{u}-\frac{1}{\xi+1-\eta}f, \qquad \bar{u}_\eta=\frac{\bar{h}(1+\xi)}{\xi+1-\eta}\bar{w}, \tag{33b), (33c}$$

where $\bar{h}(\xi)=\bar{h}(x)$ and $t=\lambda(\bar{h}(1+\xi)^{1+\beta}/(\xi+1-\eta)^3)$. Here $\alpha=\frac{1}{2}$, $\beta=0$, and $\lambda=1$ have been introduced so that Eqs. (33) will be capable of describing all four cases. Boundary conditions (26) now become

$$\begin{aligned} &f=0, \quad \bar{u}=0 \quad \text{on} \quad \eta=0,\ \xi>0\\ &f=\gamma, \quad \bar{w}=0 \quad \text{on} \quad \eta=1,\ \xi>0\\ &f=f_0(\eta) \quad \text{on} \quad \xi=0,\ 0\leqslant\eta\leqslant 1, \end{aligned} \tag{34}$$

where the initial profile $f_0(\eta)$ is found by putting $\xi=0$ and $\bar{h}=\gamma$ into (33) and solving subject to conditions $f=\bar{u}=0$ at $\eta=0$ and $f=\gamma$ at $\eta=1$. This needs to be found numerically (see next section).

Although the discrepancy in boundary conditions at (0, 0) has been removed, it will be observed that transformation (31) has a coordinate singularity at $\xi=0$, $\eta=1$ (it does not seem possible to devise a transformation with the required properties without incurring such a singularity). However, the flow is very uniform in the neighbourhood of this point and we experienced no difficulty in obtaining numerical results of high accuracy. For the flat plate case (a) $u\sim 1-e^{-k/d^2}$, where d is the distance from the singularity, which is extremely flat.

For the 2-dimensional flat plate (a) the equations are the same as the cylindrical case with the gravitational term in Eq. (25b) set to zero. In this case, however, we would like to integrate the equations over the whole range $0\leqslant\xi<\infty$ and to perform this numerically in a satisfactory manner we require the dependent variables to be of order unity throughout the entire range (see [9]). For large x the boundary condition (26) implies that ψ will be independent of x and hence (25a) will permit a similarity variable $\bar{y}/x$. Hence for large x, $\bar{h}\sim x$ and conservation of

mass demands $u \sim 1/x$. For f, $\bar{u}$, and $\bar{w}$ to be of order unity over the whole range of ξ we set

$$r = \frac{1}{(1+\xi)^2}, \qquad \bar{h} = (1+\xi)^2 \tilde{h}, \qquad g = \frac{\xi(1+\xi)^2}{\xi + 1 - \eta}. \tag{35}$$

Using (31), Eqs. (25a) transforms into (33), with $\alpha = \frac{1}{2}$, $\beta = 2$, and $\lambda = 1$, and is to be solved subject to (34).

For the axisymmetric flat plate (c) the boundary layer thickness grows like $x^{1/2}$ for small x in the y direction. Since, from (24), $\bar{y} = xy$, the thickness will grow like $x^{3/2}$ in units of $\bar{y}$ and hence an appropriate transformation to replace (31) is

$$\bar{y} = \frac{\xi \eta \bar{h}}{\xi + 1 - \eta}, \qquad x = \xi^{2/3}. \tag{36}$$

At large x (25c) will permit a similarity variable $\bar{y}/x^3$ and hence $\bar{h} \sim x^3$ with $u \sim 1/x^3$ from mass conservation. Demanding that dependent variables are of order unity for all ξ can be achieved by using (35) with ξ as defined by (36). Equation (25c) then transforms into (33) with $\alpha = \frac{3}{2}$, $\beta = 2$, and $\lambda = 1$ with boundary conditions as given by (34).

For the sphere (d) the geometry is axisymmetric and hence we employ the transformation (36) and since the range in x is finite ($0 \leqslant x \leqslant \pi$) it is appropriate to set $r = 1$, $\bar{h} = \tilde{h}$, and g given by (32) as in the cylindrical case. Substitution again yields equation (33) subject to boundary conditions (34) with $\alpha = \frac{3}{2}$, $\beta = 0$, and $\lambda = \xi^{4/3} \operatorname{cosec}^2(\xi^{2/3})$, where λ should be regarded as a geometrical factor.

In summary equations (33) subject to (34) describe all four cases and are derived from (30) using the transformation

$$\bar{y} = \frac{\xi(1+\xi)^\beta \eta \bar{h}}{\xi + 1 - \eta}, \qquad x = \xi^{1/\alpha} \tag{37}$$

with

$$r = \frac{1}{(1+\xi)^\beta}, \qquad \bar{h} = (1+\xi)^\beta \tilde{h}, \qquad g = \frac{\xi(1+\xi)^\beta}{\xi + 1 - \eta}, \tag{38}$$

where α, β, and λ are

$$\begin{aligned} &\text{(a)} \quad \alpha = \tfrac{1}{2}, \beta = 2, \lambda = 1, \\ &\text{(b)} \quad \alpha = \tfrac{1}{2}, \beta = 0, \lambda = 1, \\ &\text{(c)} \quad \alpha = \tfrac{3}{2}, \beta = 2, \lambda = 1, \text{ and} \\ &\text{(d)} \quad \alpha = \tfrac{3}{2}, \beta = 0, \lambda = \xi^{4/3} \operatorname{cosec}^2(\xi^{2/3}) \end{aligned} \tag{39}$$

for the four cases.

4. Numerical Procedure

(a) *Modification of the Box Method*

The numerical method employed is a modification of the Keller box method [10, 11]. A grid is placed on the domain $\xi \geqslant 0$, $0 \leqslant \eta \leqslant 1$, which is not assumed to be uniform, whose nodal points are

$$\begin{aligned} \xi_i &= \xi_{i-1} + k_i, \qquad i = 1, 2, ..., \\ \eta_j &= \eta_{j-1} + h_j, \qquad j = 1, 2, ..., N, \end{aligned} \tag{40}$$

where $\xi_0 = 0$, $\eta_0 = 0$, $\eta_N = 1$, and N is the number of mesh spaces in the η direction. Equation (33a) is differenced using formulas symmetric about $(\xi_{i-1} + k_i/2, \eta_{j-1} + h_j/2)$ which for any function $z(\xi, \eta)$ are

$$\begin{aligned} \frac{\partial z}{\partial \xi} &\simeq \frac{1}{2k_i}(z_{i,j} - z_{i-1,j} + z_{i,j-1} - z_{i-i,j-1}) \\ \frac{\partial z}{\partial \eta} &\simeq \frac{1}{2h_j}(z_{i,j} - z_{i,j-1} + z_{i-1,j} - z_{i-1,j-1}) \\ z &\simeq \tfrac{1}{4}(z_{i,j} + z_{i,j-1} + z_{i-1,j} + z_{i-1,j-1}), \end{aligned} \tag{41}$$

where $z_{i,j} \equiv z(\xi_i, \eta_j)$. Since (33b), (33c) do not have a ξ derivative they can be differenced about the point $(\xi_i, \eta_{j-1} + h_j/2)$. It was found in practice that this damps high frequency Fourier error components better than differencing about $(\xi_{i-1} + k_i/2, \eta_{j-1} + h_j/2)$. The appropriate formulas are given by setting index $i-1$ to i in (41).

Since the equations are parabolic a solution can be found by marching in the ξ direction. That is if all the variables are known at location $i-1$ then the difference equations resulting from (33) and (34) give a set of $3N+4$ nonlinear equations for the $3N+4$ unknowns f_{ij}, $\bar{u}_{ij}$, $\bar{w}_{ij}$, $j = 0, 1, ..., N$ and $\bar{h}_i$.

These are solved using Newton's iteration

$$\begin{aligned} A^{(s)}\, \Delta \mathbf{x}^{(s)} &= -\boldsymbol{\phi}^{(s)} \\ \mathbf{x}^{(s+1)} &= \mathbf{x}^{(s)} + \Delta \mathbf{x}^{(s)}, \qquad s = 0, 1, 2, ..., \end{aligned} \tag{42}$$

where $A^{(s)} \equiv \partial \boldsymbol{\phi}^{(s)}/\partial \mathbf{x}^{(s)}$, $\mathbf{x}^{\tau} = (f_{i0}, \bar{u}_{i0}, \bar{w}_{i0}, f_{i1}, \bar{u}_{i1} \bar{w}_{i1}, ..., f_{iN}, \bar{u}_{iN}, \bar{w}_{iN}, \bar{h}_i)$, and $\boldsymbol{\phi}$ consists of the left-hand sides of the differenced equations of (33) and (34) in which all terms have been taken over to the left. The ordering of equations in $\boldsymbol{\phi}$ is (i) boundary conditions (34) at $\eta = 0$, (ii), Eqs. (33) in the order a, b, c at the centred location $j = \frac{1}{2}, \frac{3}{2}, ..., N - \frac{1}{2}$, and (iii) conditions (34) at $\eta = 1$. For $N = 3$, $A^{(s)}$ has the form

$$\left[\begin{array}{ccc|ccc|ccc|c}
1 & 0 & 0 & & & & & & & 0 \\
0 & 1 & 0 & & & & & & & 0 \\
\hline
* & * & * & * & * & * & & & & * \\
* & * & 0 & * & * & 0 & & & & * \\
0 & * & * & 0 & * & * & & & & * \\
\hline
 & & & * & * & * & * & * & * & * \\
 & & & * & * & 0 & * & * & 0 & * \\
 & & & 0 & * & * & 0 & * & * & * \\
\hline
 & & & & & & * & * & * & * \\
 & & & & & & * & * & 0 & * \\
 & & & & & & 0 & * & * & * \\
\hline
 & & & & & & & & & 1 \quad 0 \quad 0 \quad 0 \\
 & & & & & & & & & 0 \quad 0 \quad 1 \quad 0
\end{array}\right] \tag{43}$$

where $*$ denotes a possible non-zero element and unfilled parts are zero.

Matrix (43) can be expanded by two extra rows and columns to form a block matrix with 3×3 blocks if we include two extra unknowns s_1 and s_2 and two extra equations $s_1 = 0$ and $s_2 = 0$. The dummy variables s_1, and s_2 are appended to $\mathbf{x}$ and the left-hand sides of the two dummy equations appended to $\boldsymbol{\phi}$. We now have $3N+6$ equations and unknowns and the matrix $A^{(s)}$ has the form

$$\left[\begin{array}{cccccc}
A_0 & C_0 & & & & D_0 \\
B_1 & A_1 & C_1 & & & D_1 \\
 & B_2 & A_2 & C_2 & & D_2 \\
 & & \ddots & \ddots & \ddots & \vdots \\
 & & B_{N-1} & A_{N-1} & C_{N-1} & D_{N-1} \\
 & & & B_N & A_N & D_N \\
 & & & & B_{N+1} & A_{N+1}
\end{array}\right], \tag{44}$$

where the A's, B's, C's, and D's are 3×3 matrices in which the B's, C's, and D's are respectively of the form

$$\begin{bmatrix} * & * & * \\ * & * & * \\ 0 & 0 & 0 \end{bmatrix}, \quad \begin{bmatrix} 0 & 0 & 0 \\ 0 & 0 & 0 \\ * & * & * \end{bmatrix}, \quad \begin{bmatrix} * & 0 & 0 \\ * & 0 & 0 \\ * & 0 & 0 \end{bmatrix}$$

and where

$$A_{N+1}=\begin{bmatrix}0 & 0 & 0\\ 0 & 1 & 0\\ 0 & 0 & 1\end{bmatrix}, \qquad B_{N+1}=\begin{bmatrix}0 & 0 & 1\\ 0 & 0 & 0\\ 0 & 0 & 0\end{bmatrix}. \tag{45}$$

Thus the matrix $A^{(s)}$ is not block diagonal as is usual with the Keller box method and the solution of (42) needs to be modified to take account of the column of D's. Let $\Delta\mathbf{x}^{\tau}=(\Delta\mathbf{x}_0^{\tau}, \Delta\mathbf{x}_1^{\tau}, ..., \Delta\mathbf{x}_{N+1}^{\tau})$ and $\boldsymbol{\phi}^{\tau}=(\boldsymbol{\phi}_0^{\tau}, \boldsymbol{\phi}_1^{\tau}, ..., \boldsymbol{\phi}_{N+1}^{\tau})$, where $\Delta\mathbf{x}_j$ and $\boldsymbol{\phi}_j$ are three vectors; then a suitable algorithm for solving the matrix equation in (42) is

$$\begin{gathered}
E\leftarrow A_0^{-1}, \qquad \boldsymbol{\phi}_0\leftarrow \mathbf{E}_0, \qquad D_0\leftarrow ED_0\\
A_{j-1}\leftarrow EC_{j-1}, \qquad E\leftarrow (A_j-B_jA_{j-1})^{-1}\\
\boldsymbol{\phi}_j\leftarrow E(\boldsymbol{\phi}_j-B_j\boldsymbol{\phi}_{j-1}), \qquad D_j\leftarrow E(D_j-B_jD_{j-1}), \qquad j=1, 2, ..., N\\
A_N\leftarrow D_N, \qquad E\leftarrow (A_{N+1}-B_{N+1}A_N)^{-1}\\
\Delta\mathbf{x}_{N+1}\leftarrow E(\boldsymbol{\phi}_{N+1}-B_{N+1}\boldsymbol{\phi}_N)\\
\Delta\mathbf{x}_N\leftarrow \boldsymbol{\phi}_N-A_N\Delta\mathbf{x}_{N+1}\\
\Delta\mathbf{x}_j\leftarrow \boldsymbol{\phi}_j-A_j\Delta\mathbf{x}_{j+1}-D_j\Delta\mathbf{x}_{N+1}, \qquad j=N-1, N-2, ..., 0,
\end{gathered} \tag{46}$$

where $\leftarrow$ denotes replacement. Algorithmically this is simply a modification of the usual solution of a block tridiagonal system to include the D_j. The algorithm can be made efficient by taking account of the zeros appearing in matrices (45).

For the initial profile $f_0(\eta)$, $\xi=0$ and $\tilde{h}=\gamma$ in Eq. (33) and, since no ξ derivatives appear, (33a) is differenced the same way as (33b, 33c). The ensuring system reduces to $3N+3$ equations and unknowns which are solved using (42). In this case $A^{(s)}$ is block tridiagonal and can be inverted in the usual way.

(b) *Extrapolating the Results*

Since central differences are used, the local truncation error can be written as a Taylor series in powers of h^2 and k^2, where $h=\max_j h_j$ and $k=\max_i k_i$. As pointed out by Keller it is therefore possible, by solving the problem on different sized grids and using Richardson's extrapolation, to produce results of high accuracy. For example, results using $M\times N$, $2M\times 2N$, and $3M\times 3N$ grid spaces, which have local error $O(h^2+k^2)$, can be combined to produce results of $O(h^6+k^6)$ on the coarsest grid. For most problems this gives adequate highly accurate results [9, 12, 13], but for some problems, for example, jet problems [14, 15], difficulties can arise particularly near $\xi=0$. Second, if the results obtained are not sufficiently accurate it is unclear which of h or k needs to be reduced. For these reasons we adopt the following approach.

Suppose a coarse grid of size $M\times N$ is placed on the ξ, η domain with each cell being divided into n_i and m_j sub-cells in the ξ and η directions, respectively, and the

TABLE I

The Extrapolation Process for the Film Thickness at $\xi = 1$ in the cylindrical case $F = 2, \gamma = 1$

$\xi - \eta$ extrapolation			$\eta - \xi$ extrapolation		
	(a)			(b)	
2.0104300			2.0104300		
2.0099066	2.0097321		2.0102938	2.0101847	
2.0098107	2.0097340	2.0097343	2.0102468	2.0101865	2.0101871
2.0102938			2.0099066		
2.0097696	2.0095949		2.0097696	2.0096600	
2.0096736	2.0095968	2.0095971	2.0097229	2.0096628	2.0096637
2.0102468			2.0098107		
2.0097229	2.0095482		2.0096736	2.0095639	
2.0096269	2.0095502	2.0095504	2.0096269	2.0095669	2.0095679
	(c)			(d)	
2.0097343			2.0101871		
2.0095971	2.0094873		2.0096637	2.0094893	
2.0095504	2.0094905	2.0094915	2.0095679	2.0094913	2.0094915

problem is solved numerically for each of the cases $i = 1, 2, 3$ and $j = 1, 2, 3$. If the set $\{g_{ij}\}$ denotes the result at a common grid point then g_{1j}, g_{2j}, and g_{3j} give an extrapolated result $\bar{g}_j$ which has error $O(h^2 + k^6)$ given by

$$\bar{g}_j = \frac{n_3^2 h_{23} - n_1^2 h_{12}}{n_3^2 - n_1^2}; \qquad h_{12} = \frac{n_2^2 g_{2j} - n_1^2 g_{1j}}{n_2^2 - n_1^2}, \qquad h_{23} = \frac{n_3^2 g_{3j} - n_2^2 g_{2j}}{n_3^2 - n_2^2}. \tag{47}$$

This is illustrated for a typical variable by (a) in Table I in which column 1 contains the g_{ij}, column 2 the elements h_{12}, h_{23}, and column 3 the $\bar{g}_j$. The $\bar{g}_j$ are then used to give a final extrapolated result $\bar{g}$ with error $O(h^6 + k^6)$ using formulae similar to (47) with n_i replaced by m_j ((c) in Table I). One may obtain $\bar{g}$ by a different route, namely, using g_{i1}, g_{i2}, and g_{i3} we can obtain extrapolated results $\bar{g}_i$ which are $O(h^6 + k^2)$ and then extrapolating the $\bar{g}_i$ finally gives $\bar{g}$ ((b) and (d) in Table I). The $\bar{g}_j$, being $O(h^2 + k^6)$, are virtually error free from the ξ discretisation and the differences between them reflect the error due to the η discretisation. Similarly, the $\bar{g}_i$ reflect the error due to the ξ discretisation and, hence, it is possible to decide which of either h or k needs to be reduced if more accuracy is required. The acquisition of nine sets of results rather than three obviously involves more computer time, but the added flexibility and robustness of method more than compensates for this, especially since the total time taken is not long on modern machines.

In order to estimate the error we assume that $|\bar{g}_3 - h_{23}|$, $|h_{23} - \bar{g}|$, and $|\bar{g} - g|$ are roughly geometric where g is the true solution. This is obviously crude but experience has shown that this gives the order of magnitude of the error more

accuratemy than $|h_{23} - \bar{g}|$. Applying this to both $\bar{g}_i$ and $\bar{g}_j$ gives errors in the results from the ξ and η discretisations, respectively; the maximum of the two can be taken as the error incurred.

(c) *Separation in the Cylindrical Case*

In the case of the cylinder it is conceivably possible to place a vertical barrier at the top generator which only allows fluid to pass around one side of the cylinder. Hence instead of two films colliding at $x = \pi$, the one film would continue past π and leave the surface at some point $\pi + x_1$ ($x_1 > 0$). At this separation point the skin friction is zero; that is, $u_y = 0$ at $x = \pi + x_1$, $y = 0$. Since the equations become singular at this point, the point is approached geometrically in the following manner. If ξ_s is the separation point and $\tilde{w} = \bar{w}(\xi, 0)$ then a feature for boundary layer separation is that $\tilde{w}$ is proportional to $(\xi_s - \xi)^{1/2}$ near separation. Thus if the equations have been integrated as far as ξ_n and assuming that $(\xi_s - \xi_n)$ is proportional to $\tilde{w}_n^2$ then

$$\xi_s \simeq \xi_s^n = \xi_n + (\xi_n - \xi_{n-1}) \frac{\tilde{w}_n^2}{\tilde{w}_{n-1}^2 - \tilde{w}_n^2}. \tag{48}$$

The new value ξ_{n+1} is given dynamically by $\xi_n + c(\xi_n^n - \xi_n)$, where $0 < c < 1$; the value of c used in the calculations is 0.4. Using this technique we were able to integrate to within 10^{-10} of separation. Since the ξ_n are given dynamically they need to be subjected to the extrapolation process described earlier so both the ξ coordinate and ξ_s are accurate to $O(h^6 + k^6)$.

In the spherical case the geometical factor $\lambda \to \infty$ as $x \to \pi$. In order to maintain accuracy it is necessary to approach $x = \pi$ with increasingly shorter step-lengths, and a geometric decrease accomplishes this satisfactorily.

5. Results and Conclusions

A typical run had a coarse grid of dimensions 60×48 on the (ξ, η) domain with each cell being divided into 1, 2, 3 and 2, 3, 4 sub-cells for the two directions, respectively. Because of the coordinate singularity at $\xi = 0$, $\eta = 1$ a non-uniform grid was employed given by (a) $\xi = \frac{1}{3}\sinh[\bar{\xi}^{1.5}(1 + \bar{\xi}^{1.5})]$, (b) $\xi = \bar{\xi}^{1.5}$, (c) and (a), and (d) $\xi = \bar{\xi}^{1.75}$ with $\eta = 1 - (1 - \bar{\eta})^{1.5}$ for each case where $\bar{\xi}$ and $\bar{\eta}$ are uniform. This gave $\Delta\xi \sim 0.004$ and $\Delta\eta \sim 0.003$ near the singularity in all cases, which is sufficiently small to give good accuracy. The formulae in (a) and (c) enabled us to integrate as far as $\xi \sim 10^9$, which was necessary for the profile at infinity to be determined with sufficient accuracy. The programs were run on a VAX 8650 and each took approximately 6–7 min of CPU time.

From the convergence of the extrapolation process described in the last section the absolute errors for the four cases are (a) 3×10^{-7}, (b) 2×10^{-7}, (c) 9×10^{-7}, and (d) 6×10^{-7}. Comparing the initial profile at $\xi = 0$ with the Blasius solution,

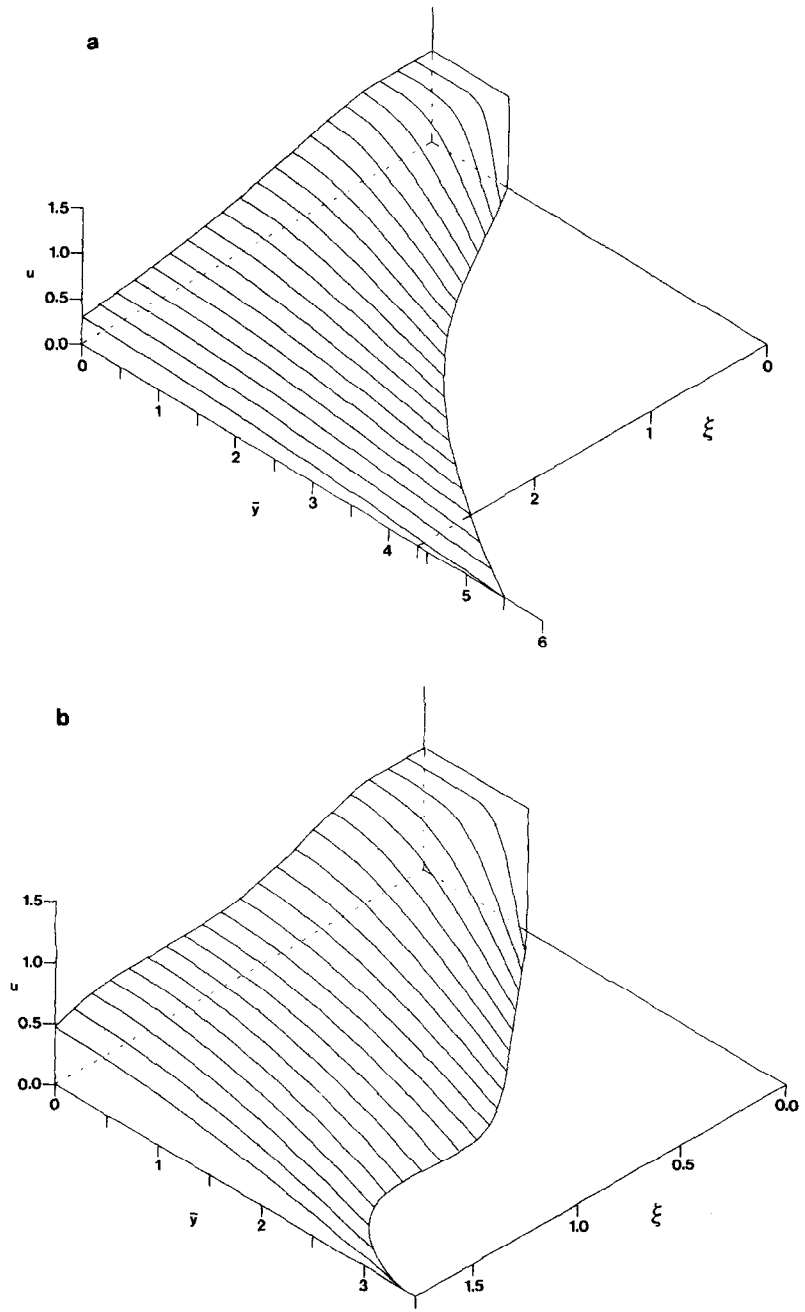

FIG. 2. Velocity profiles for (a) the 2-dimensional flat plate; (b) the cylinder, $F=5$, $\gamma=1$; (c) the axisymmetric flat plate; and (d) the sphere, $F=10$, $\gamma=\frac{1}{2}$. The outer edge of the profiles are aligned along the ξ-axis.

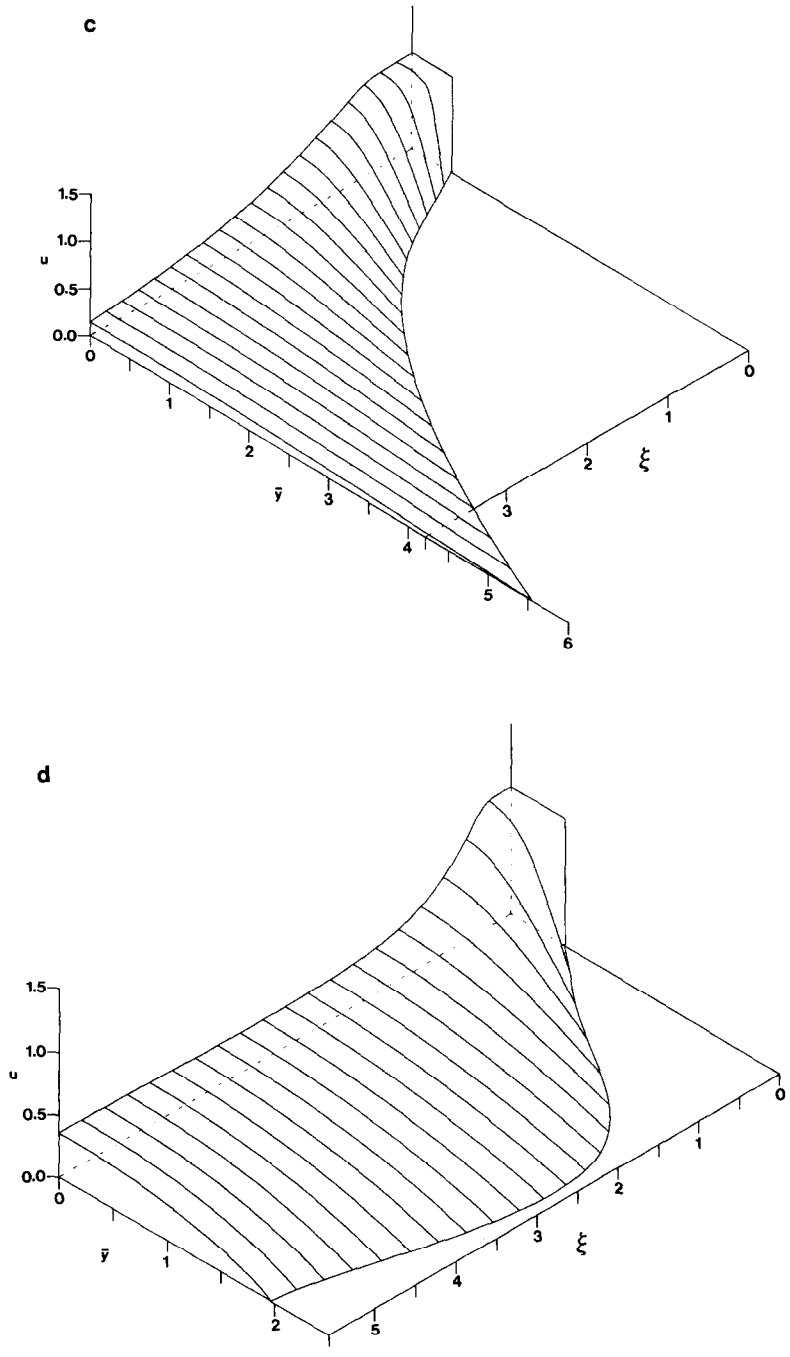

FIG. 2—*Continued.*

it is found to be accurate to at least seven decimal places. For the two flat plate cases, the solution as $\xi \to \infty$ is known [1] and this indicates an accuracy of seven or eight decimal places. From this data the results seem accurate to about six decimal places which is more than sufficient for most purposes.

Figures 2–7 depict the flavour of the results. Figure 2 shows isometric type plots of the velocity profiles $u(\xi, \bar{y})$, $0 \leqslant \bar{y} \leqslant \bar{h}$, on the ξ, $\bar{y}$ plane. These have been shifted in the $\bar{y}$ direction such that the outer edge lies along the ξ axis in order to facilitate easier viewing. The curves joining the profiles are thus the edge velocity $u(\xi, \bar{h})$ and the scaled film thickness $\bar{h}$. The individual cases shown are (a) the 2-dimensional flat plate, (b) the cylinder $F = 5$, $\gamma = \frac{1}{2}$, (c) the axisymmetric flat plate, and (d) the sphere $F = 10$, $\gamma = \frac{1}{2}$. Table II gives the numerical results for the scaled film thickness and edge velocity in these four cases. Figures 3–7 show (a) the scaled film thickness and (b) the edge velocity for various cases. Figure 3 shows the two flat plate cases, Figs. 4–6 show the cylindrical results for $\gamma = 1$, 0.5, and 0.2 respectively for each of the cases $F = 1$, 2, 5, and 10, and finally Fig. 7 shows the sphere for $\gamma = \frac{1}{2}$ with the same four values of F.

In the two flat plate cases (Fig. 3) we see, as expected, the viscosity slows down the flow such that, at large x, the velocity varies as $1/x$ for the 2-dimensional case and $1/x^3$ for the axisymmetric case as anticipated by the theory. The film thickness

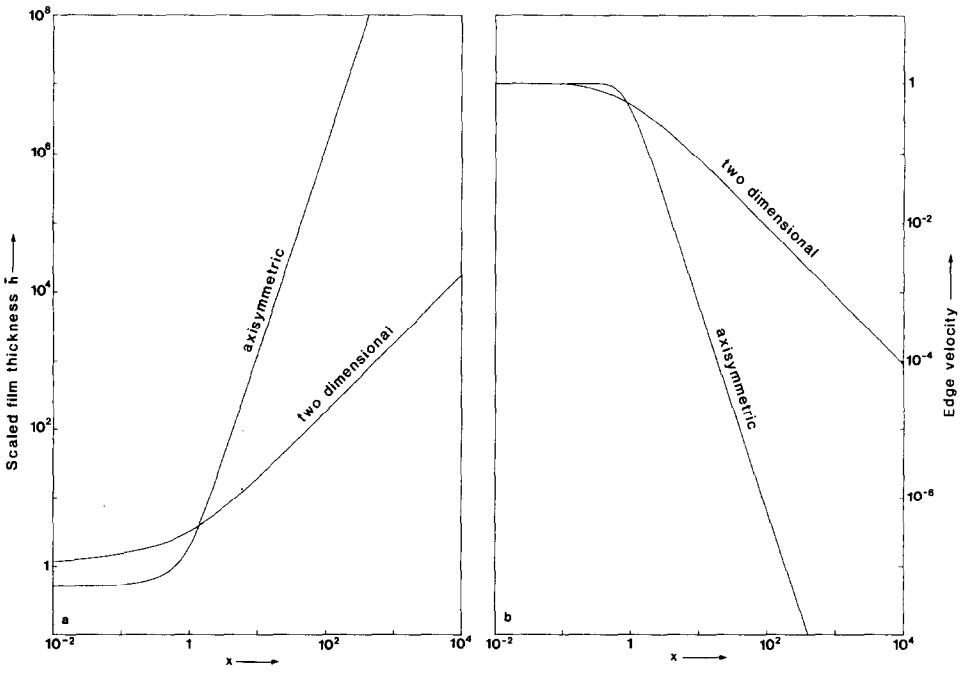

FIG. 3. (a) Scaled film thickness and (b) edge velocity for the 2-dimensional and axisymmetric flat plates.

TABLE II(a)

Film Thickness and Edge Velocity
for the 2-Dimensional Flat Plate

x	Film thickness	Edge velocity
0.0	1.000000	1.000000
0.01	1.172079	1.000000
0.05	1.384780	0.9987022
0.2	1.774921	0.9009388
[illegible]	[illegible]	[illegible]
2.0	5.057765	0.3214787
5.0	10.49916	0.1548660
10.0	19.56816	0.08309232
30.0	55.84414	0.02236693
100.0	182.8101	8.894277×10^{-3}
400.0	726.9498	2.236693×10^{-3}
2×10^3	3.629029×10^3	4.480438×10^{-4}
1×10^4	1.813942×10^4	8.963701×10^{-5}
1×10^5	1.813814×10^5	8.964337×10^{-6}
1×10^7	1.813799×10^7	8.964408×10^{-8}
1×10^9	1.813799×10^5	8.964408×10^{-10}

TABLE II(b)

Film Thickness and Edge Velocity for the Cylinder $F = 5$, $\gamma = \frac{1}{2}$

x	Film thickness	Edge velocity
0.0	0.5000000	1.000000
0.01	0.6720672	0.9996728
0.03	0.7980861	0.9653357
0.06	0.9265360	0.8687237
0.1	1.074188	0.7550066
0.2	1.419663	0.5694673
0.3	1.726205	0.4638910
0.5	2.129748	0.3641918
0.7	2.237806	0.3371484
1.0	2.145926	0.3470054
1.3	2.032394	0.3669183
1.6	1.975079	0.3788947
2.0	1.991970	0.3774695
2.5	2.188305	0.3464769
3.0	2.829822	0.2753540
π	3.287692	0.2437365

TABLE II(c)

Scaled Film Thickness and Edge Velocity for the Axisymmetric Flat Plate

x	Scaled film thickness	Edge velocity
0.0	0.5000000	1.000000
0.1	0.5314171	1.000000
0.2	0.5888611	1.000000
0.3	0.6632482	0.9998393
0.4	0.7513553	0.9870793
0.5	0.8523836	0.9285230
0.7	1.129381	0.7193735
1.0	1.924282	0.4224856
1.5	4.796132	0.1695078
2.0	10.38868	0.07825651
3.0	33.36347	0.02436742
5.0	151.8650	5.353319×10^{-3}
10.0	1.209914×10^{3}	6.719332×10^{-4}
20.0	9.674311×10^{3}	8.403511×10^{-5}
50.0	1.511506×10^{3}	5.378619×10^{-6}
100.0	1.209200×10^{6}	6.723302×10^{-7}
1×10^{3}	1.209200×10^{9}	6.723307×10^{-10}
1×10^{4}	1.209199×10^{12}	6.723306×10^{13}

TABLE II(d)

Scaled Film Thickness and Edge Velocity for the Sphere $F = 10, \gamma = \frac{1}{2}$

x	Scaled film thickness	Edge velocity
0.0	0.5000000	1.000000
0.2	0.5871499	1.001992
0.4	0.7395193	0.9961222
0.6	0.9301206	0.8619230
0.8	1.195809	0.6709312
1.0	1.538011	0.5163180
1.2	1.884614	0.4149664
1.4	2.155804	0.3570408
1.6	2.320050	0.3277185
1.8	2.392590	0.3152320
2.0	2.400636	0.3124411
2.3	2.333868	0.3189425
2.6	2.206407	0.3333528
3.0	2.005745	0.3536769
π	1.95855	0.35609

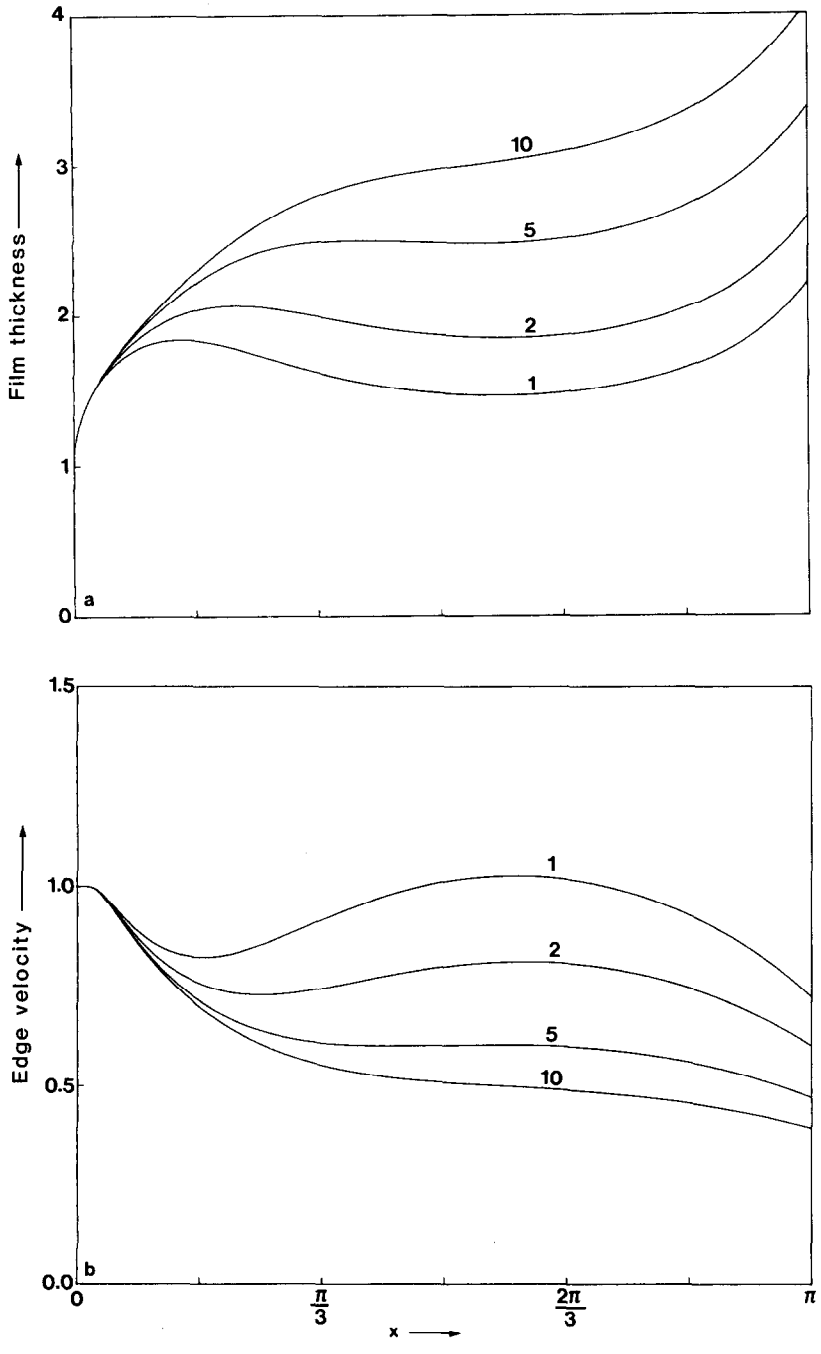

FIG. 4. (a) Film thickness and (b) edge velocity for the cylinder with $\gamma = 1$ for various values of F.

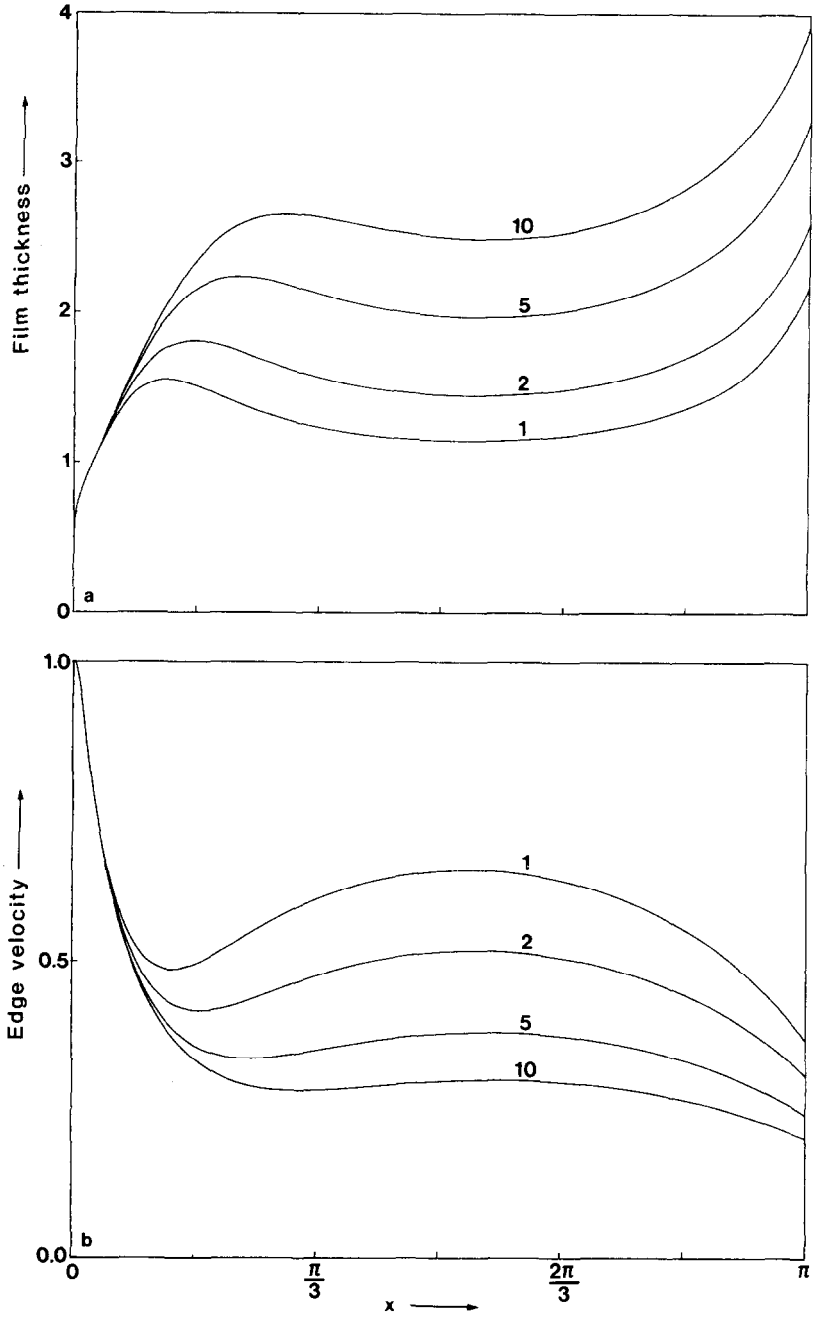

FIG. 5. (a) Film thickness and (b) edge velocity for the cylinder with $\gamma = 0.5$ for various values of F.

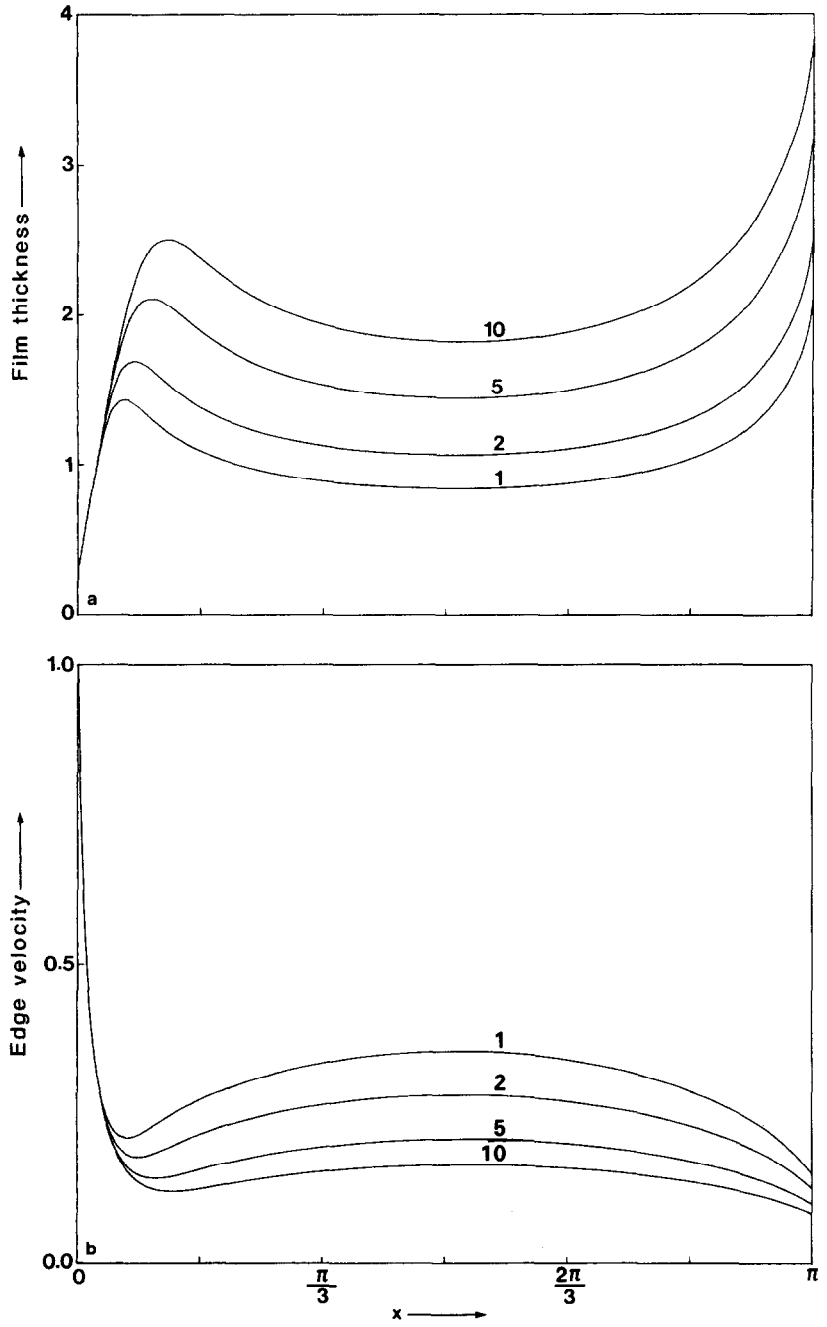

FIG. 6. (a) Film thickness and (b) edge velocity for the cylinder with $\gamma = 0.2$ for various values of F.

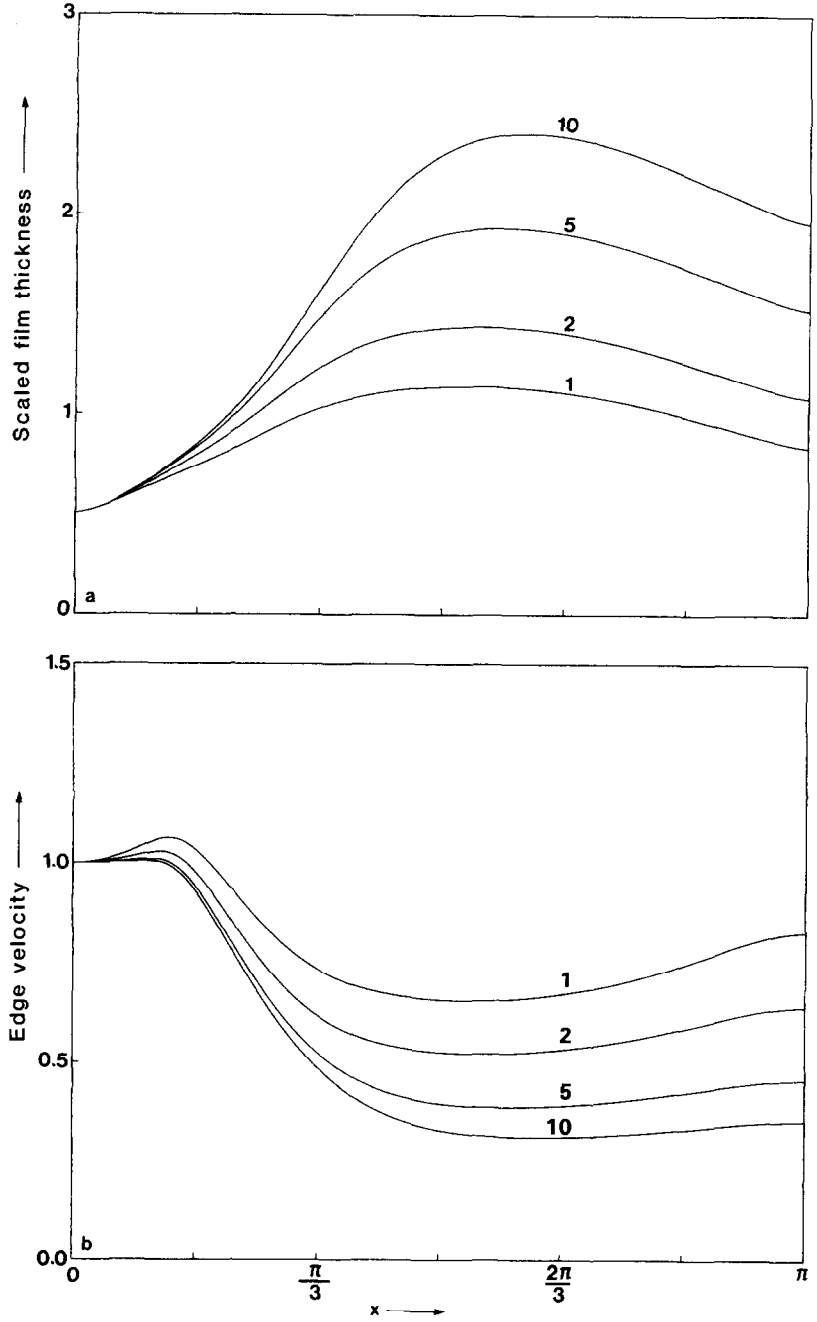

FIG. 7. (a) Scaled film thickness and (b) edge velocity for the sphere with $\gamma = \frac{1}{2}$ for various values of F.

increases with x (a consequence of the conservation of mass) with h varying as x and x^2 for the two cases, respectively ($\bar{h}$ varies as x^3 in the axisymmetric case). For the cylindrical cases (Figs. 4–6), the velocity of the flow is controlled by two opposing forces, viscosity trying to slow it down and gravity trying to speed it up. The gravitational component of force affecting the flow is greatest near $x = \pi/2$ and least near $x = 0$ and $x = \pi$. Hence initially we have a decrease in velocity (which is sharp in most cases), followed by a slight increase as gravity starts to dominate, and finally a gradual decrease as the bottom generator is approached. As F increases the effect of gravity decreases and hence the high velocity results correspond to the small F values. As γ decreases the amount of fluid in the impinging jet decreases and the thinner the ensuing film. In such cases the boundary layer will reach the outer boundary (point B in Fig. 1(b)) sooner and hence the initial velocity decrease becomes more sharp as γ decreases. Owing to mass conservation the film thickness curves vary in an analogous but opposite sense to those of the edge velocity. Because of the geometrical effect, the spherical edge velocity (Fig. 7) is initially affected mainly by gravity with the decrease in velocity due to viscosity occurring later.

For the cylinder, where the flow is restricted to one side, the separation points obtained were found to be accurate to six decimal places and the values of x_1 for $\gamma = 1$ are shown in the table below. For the higher gravity dominated cases (small F),

F	1	2	5	10
x_1	0.221636	0.260809	0.322047	0.379619

the flow separates sooner as one would expect intuitively.

It is not the intention in this paper to make formal comparisons with the theoretical results obtained using integral methods since this has been done elsewhere [8]. However, in the summary of that paper it was found that good agreement is obtained in all cases where the Pohlhausen technique is used with an assumed quadratic fit for the velocity profile. Even better agreement is obtained for quartic profiles including a good prediction of the separation point for the one-sided flow around a cylinder. Hence one can use the Pohlhausen method for similar problems with a high degree of confidence especially if quartic velocity profiles are assumed.

In conclusion we have demonstrated that by modifying the Keller box method it is possible, incorporating extrapolation, to obtain results of high accuracy for parabolic problems having a free boundary. Furthermore it is possible to successfully remove the singularity associated with the leading edge of the boundary layer equations and simultaneously keep the outer boundary at a finite distance from the generating surface. The technique can be used as the basis of more complex problems, for example, thermal and convective layers and truly 3-dimensional flows such as an axisymmetric vertical jet impinging on the top generator of a cylinder.

ACKNOWLEDGMENT

I thank Professor Graham Wilks for introducing me to this problem and for his constant help and encouragement.

REFERENCES

1. E. J. WATSON, *J. Fluid Mech.* **20**, 481 (1964).
2. S. H. SMITH, *J. Eng. Math.* **5**, 11 (1971).
3. J. H. MERKIN, *J. Eng. Math.* **7**, 319 (1973).
4. A. SOLAN AND A. ZFATI, in *Proceedings, Fifth International Heat Transfer Conference, Tokyo, 1974.*
5. R. J. GRIBBEN, in *Math. Eng. Ind.*, in press.
6. M. A. ABDELGHAFFER, A. A. NICOL, R. J. GRIBBEN AND G. WILKS, to be published in *Math. Eng. Ind.* in press.
7. L. ROSENHEAD (Ed.), *Laminar Boundary Layers* (Oxford Press (Clarendon), London/New York, 1963).
8. R. J. GRIBBEN, R. HUNT, M. A. ABDELGHAFFAR, AND G. WILKS, *Appl. Math. Modelling*, in press.
9. J. CRANK, *Free and Moving Boundary Problems* (Oxford Press (Clarendon), London/New York, 1984).
10. R. HUNT AND G. WILKS, *J. Comput. Phys.* **40**, 478 (1981).
11. H. B. KELLER AND T. CEBECI, in *Proceedings, Second International Conference on Numerical Methods in Fluid Dynamics, Berkeley, California, 1971.*
12. H. B. KELLER, *Ann. Rev. Fluid Mech.* **10**, 417 (1978).
13. R. HUNT AND WILKS, *J. Fluid Mech.* **101**, 377 (1980).
14. G. WILKS AND R. HUNT, *J. Appl. Math. Phys.* **35**, 34 (1984).
15. G. WILKS AND R. HUNT, *Proc. R. Soc. Edinburgh A* **90**, 13 (1981).
16. G. WILKS, R. HUNT, AND D. S. RILEY, *Num. Heat Transfer* **8**, 179 (1985).